Production and constraints for a massive dark photon at electron-positron colliders*

Jun Jiang(蒋军)[1;1]   Chun-Yuan Li(李春园)[1;2]   Shi-Yuan Li(李世渊)[1;3]   Shankar Dayal Pathak[1,2;4]

Zong-Guo Si(司宗国)[1;5]   Xing-Hua Yang(杨兴华)[1;6]

[1]School of Physics, Shandong University, Jinan, Shandong 250100, China
[2]Department of Physics, Lovely Professional University, Phagwara, Punjab, 144411, India

Abstract: Dark sector may couple to the Standard Model via one or more mediator particles. We discuss two types of mediators: the dark photon A' and the dark scalar mediator ϕ. The total cross-sections and various differential distributions of the processes $e^+e^- \to q\bar{q}A'$ and $e^+e^- \to q\bar{q}\phi$ ($q = u$, d, c, s and b quarks) are discussed. We focus on the study of the invisible A' due to the cleaner background at future e^+e^- colliders. It is found that the kinematic distributions of the two-jet system could be used to identify (or exclude) the dark photon and the dark scalar mediator, as well as to distinguish between them. We further study the possibility of a search for dark photons at a future CEPC experiment with $\sqrt{s} = 91.2$ GeV and 240 GeV. With CEPC running at $\sqrt{s} = 91.2$ GeV, it would be possible to perform a decisive measurement of the dark photon (20 GeV $< m_{A'} < 60$ GeV) in less than one operating year. The lower limits of the integrated luminosity for the significance $S / \sqrt{B} = 2\sigma$, 3σ and 5σ are presented.

Keywords: dark photon, dark scalar mediator, CEPC

1   Introduction

Signals of non-baryonic dark matter (DM) in the Universe have been identified in a number of astrophysical and cosmological observations, such as the Cosmic Microwave Background anisotropy measurements, galactic rotation curves, large scale structure surveys, X-ray observations and gravitational lensing [1-11]. The contribution of DM is nearly 75% of the total matter in the Universe. Specifically, the Planck data give the value of the relic density of DM of $\Omega_{CDM}h^2 = 0.120 \pm 0.001$ [1]. DM influences the dynamical effects from the scale of a galaxy up to the cosmic scale, and plays a crucial role in the galaxy rotation curve and the formation of structures in the Universe. However, the nature of the DM particles remains a mystery and has become one of the most im-

portant challenges of modern science. The underlying physics of DM particles is explored by various worldwide projects, such as the direct and indirect searches, collider experiments and astrophysical signatures arising from DM self-interactions [12-15].

Given the intricate structure of the Standard Model (SM), which describes only a sub-dominant component of the Universe, it would not be surprising if the dark sector contains itself a rich structure, with DM making only a part of it. In the dark sector, the DM particles do not interact directly with the known forces, except with the gravitational force. However, there are typically one or more mediator particles which are coupled with SM and act as a "portal" [16-21]. Such extended interactions associating the dark sector and SM depend on the spin and parity: the mediators can be vector A', scalar ϕ, pseudo-

scalar a, axial-vector Z' and even fermions N.

A new force mediated by dark photons has been a subject of considerable interest in high energy physics. The existence of the dark photon [22-24], associated to a hidden $U(1)'$ gauge interaction, has been the subject of many investigations, both theoretical and experimental. Substantial effort has been invested in the search for dark photons using various processes including bremsstrahlung $e^-Z \to e^-ZA'$ [25-28], meson decays $\pi^0/\eta/\eta' \to \gamma A'$, $K \to \pi A'$, $\phi \to \eta A'$ and $D^* \to D^0 A'$ [29-31], the Drell-Yan process $q\bar{q} \to A' \to (\ell^+\ell^-$ or $h^+h^-)$ [32,33], annihilation $e^+e^- \to \gamma A'$ [34-38], etc. Stringent limits for the kinetic mixing parameter ε for a given dark photon mass $m_{A'}$ have been obtained [17,18,24,39,40]. For $m_{A'} \lesssim 1$ GeV, only limited values of ε are allowed. However, for a heavy dark photon, a wide range of mixing parameter values has not been excluded by the current experiments.

Future high-energy electron-positron colliders provide an opportunity to search for the dark sector mediators. These colliders include CEPC [41], ILC [42], FCC-ee [43] and CLIC [44], with the center-of-mass energy $\sqrt{s}$ varying from 91.2 GeV to 1 TeV. Assuming that dark mediators interact only with quarks, we investigate in this work the production of dark photon A' and dark scalar mediator ϕ at electron-positron colliders with $\sqrt{s}$ = 91.2 GeV, 240 GeV, 500 GeV and 1 TeV. We analyze the cross-sections and the normalized kinematic distributions of the processes $e^+e^- \to q\bar{q}A'$ and $e^+e^- \to q\bar{q}\phi$, and focus on the invisible A' due to a cleaner background. The corresponding background processes are also simulated.

The paper is organized as follows. In Sec. 2, we present a simple theoretical framework for the dark photon and dark scalar mediator. In Sec. 3, we investigate the production of dark photon and dark scalar mediator at future e^+e^- colliders, and discuss how to distinguish between them. In Sec. 4, we study the discovery potential of dark photons at a CEPC experiment. Finally, a short summary is given.

2   Dark photon and dark scalar mediator

In a simple extension of SM, one can introduce a $U(1)'$ as an extra gauge group. The gauge boson A' arises from the extra $U(1)'$ gauge group, which can be coupled weakly to electrically charged particles by "kinetic mixing" with the photon [22-24]. Kinetic mixing produces an effective parity-conserving interaction $\varepsilon e A'_\mu J^\mu_{EM}$ of A' with the electromagnetic current J^μ_{EM}, suppressed relative to the electron charge by the parameter ε [18]. The gauge boson or dark photon A' play the role of the "vector portal" connecting the SM and DM particles. We assume that the dark photon only interacts with the DM particles

and SM quarks. After diagonalization of the kinetic mixing term, the Lagrangian of the dark photon model is [19-21]

$$\mathcal{L} \supset \sum_q \bar{q}(-ec_q\gamma^\mu A_\mu - \varepsilon ec_q\gamma^\mu A'_\mu - m_q)q + \bar{\chi}(-g_\chi\gamma^\mu A'_\mu - m_\chi)\chi$$
$$- \frac{1}{4}F_{\mu\nu}F^{\mu\nu} - \frac{1}{4}F'_{\mu\nu}F'^{\mu\nu} + \frac{1}{2}m^2_{A'}A'^2, \quad (1)$$

where m_q, m_χ and $m_{A'}$ denote the masses of SM quarks, DM particle and dark photon, respectively. c_q is the charge of the quarks. $F^{\mu\nu}$ and $F'^{\mu\nu}$ are the field strengths of the ordinary photon A and the dark photon A', ε is the kinetic mixing parameter in the physical basis, g_χ is the coupling parameter between the dark photon and the dark sector, and $\alpha_\chi = g^2_\chi/(4\pi)$ is the dark fine structure constant.

A number of experiments have proposed restrictions on the mixing parameter ε [17,18,24,39]. However, for the dark photon mass $m_{A'} > 1$ GeV, a wide range of mixing parameter values has still not been excluded by the current experiments. We can extract the maximum value of ε from the direct DM detection experiments. The differential cross-sections for DM particle-nucleon scattering in the non-relativistic limit can be written as [24,45,46]

$$\frac{d\sigma}{dE_R}(v_{DM}, E_R) = \frac{8\pi\alpha_{em}\alpha_\chi\varepsilon^2 m_T}{(2m_T E_R + m^2_{A'})^2}\frac{1}{v_{DM}}Z^2_T F^2(2m_T E_R), \quad (2)$$

where E_R is the nuclear recoil energy, v_{DM} is the velocity of the DM particle in the nucleon rest frame, $\alpha_{em} = e^2/4\pi$ is the electromagnetic fine structure constant, m_T is the mass of the target nucleus, Z_T is the number of protons in the target nuclei, and $F(2m_T E_R)$ is the Helm form factor [47,48]. The dark fine structure constant α_χ can be determined from the relic abundance of DM. When m_χ is determined, the combined coupling parameter $\alpha_\chi\varepsilon^2$ can be constrained from the experimental data by evaluating the function $\chi^2 = -\sum 2\ln\mathcal{L}'$, where $\mathcal{L}'$ is the likelihood function [49,50]. Fig. 1 shows the 90% C.L. upper limits of the combined parameter $\alpha_\chi\varepsilon^2$ with m_χ = 8.6 GeV (CDMS-II-Si favors a DM mass of $m_\chi \sim 8.6$ GeV [51]), and m_χ =100 GeV constrained by the CDEX-10 [52], PandaX-II [53], DarkSide-50 [54] and XENON-1T [55] data.

Alternatively, in the dark scalar mediator ϕ model, the DM particles χ can interact with the SM particles through the "Higgs portal" [19,20]. The corresponding Lagrangian can be written as,

$$\mathcal{L} \supset \frac{1}{2}(\partial_\mu\phi)^2 - \frac{1}{2}m^2_\phi\phi^2 + \bar{\chi}(i\partial_\mu\gamma_\mu - m_\chi - \lambda_\chi\phi)\chi$$
$$- \lambda_1\upsilon\phi\left(H^+H - \frac{\upsilon^2}{2}\right) - \lambda_2\phi^2\left(H^+H - \frac{\upsilon^2}{2}\right) - V(\phi), \quad (3)$$

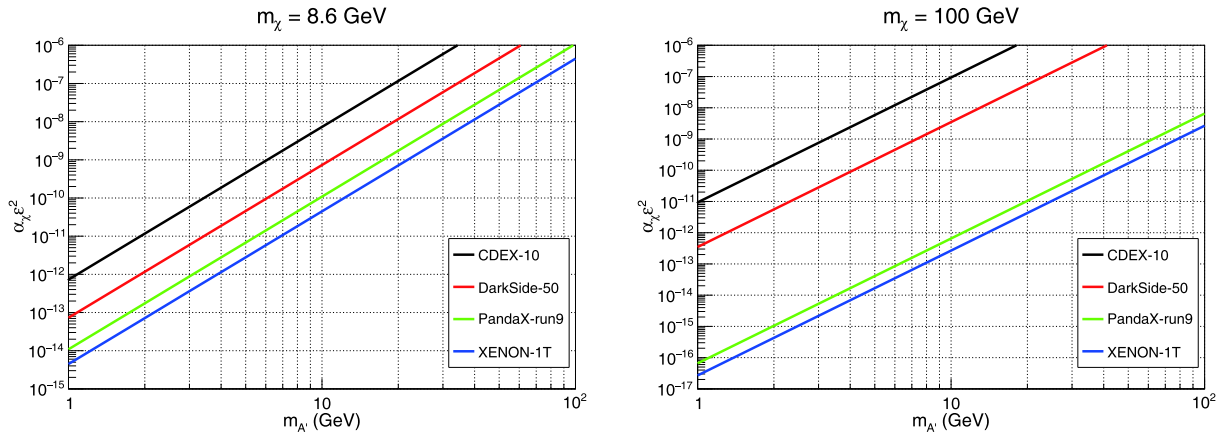where H is the SM Higgs doublet, υ is the corresponding

Fig. 1.   (color online) The 90% C.L. upper limits of the combined parameter $\alpha_\chi \varepsilon^2$ with m_χ = 8.6 GeV (left panel), and 100 GeV (right panel) from the CDEX-10 [52], PandaX-II [53], DarkSide-50 [54] and XENON-1T [55] experiments.

vacuum expectation value, and λ_χ, λ_1, λ_2 are three parameters. In the case of $\langle \phi \rangle = 0$ and $\lambda_2 \to 0$, after electroweak symmetry breaking, the relevant DM and mediator Lagrangian takes the following form,

$$\mathcal{L} \supset \frac{1}{2}(\partial_\mu \phi)^2 - \frac{1}{2}m_\phi^2 \phi^2 + \bar{\chi}(i\partial_\mu \gamma_\mu - m_\chi - \lambda_\chi \phi)\chi - \lambda_1 v^2 \phi h, \quad (4)$$

where the interaction between SM particles and DM particles are mediated by Higgs-singlet mixing, i.e., the $h - \phi$ scalar exchange. We assume that the dark scalar mediator ϕ directly couples to the SM quarks q. The dark scalar mediator plays a crucial role in the "scalar portal". The mixing term can be written as $-\varepsilon_s e \phi q \bar{q}$. We choose $\varepsilon_s = \varepsilon$ for simplicity.

3   Production of dark photon and dark scalar mediator

In this section, we investigate the production of the massive dark photon A' and of the massive dark scalar mediator ϕ via the processes $e^+e^- \to q\bar{q}A'$ and $e^+e^- \to q\bar{q}\phi$ ($q = u$, d, s, c and b) at the center-of-mass energies $\sqrt{s} =$ 91.2 GeV, 240 GeV, 500 GeV and 1 TeV, with different values of $m_{A'}$ and m_ϕ. The Feynman diagrams for the production of A' and ϕ associated with two jets at e^+e^- colliders are shown in Fig. 2.

In order to obtain the analytical amplitudes, we use FeynArts [56] and FeynCalc [57] to generate the Feynman diagrams and perform the calculations. We use the multidimensional numerical integration package Cuba

[58] to analyze the kinematic distributions. The cross-sections of the processes $e^+e^- \to q\bar{q}A'$ ($e^+e^- \to q\bar{q}\phi$) are suppressed by factors of ε^2 (ε_s^2). In order to see the general trend, we show the reduced cross-sections of the two processes as function of $\sqrt{s}$ and $m_{A'}$ or m_ϕ in Fig. 3. Fig. 3 (a) and (b) exhibit peaks due to the contribution from the resonant Z^0 boson production. Taking $m_{A'} = 20$ GeV as an example, the cross-section decreases by about three orders of magnitude when $\sqrt{s}$ increases from 91.2 GeV to 1 TeV. Fig. 3 (c) and (d) show that the reduced cross-sections become smaller as the mass becomes bigger. It is worth noting that since the value of the coupling parameter ε (ε_s) varies with the mass $m_{A'}$ (m_ϕ), the shape of the cross-section changes with $m_{A'}$ (m_ϕ) when the mass dependent ε (ε_s) is used. As we focus on the production of invisible dark photons A' and dark scalar mediators ϕ at e^+e^- colliders, one can identify them by reconstructing the missing momentum, i.e. the recoil of two final jets. The four-momentum of the two-jet system is used to infer the characteristics of the two processes. Fig. 4 shows the normalized P_T^{jj}, M_{jj}, $\cos\theta_{jj-z}$ and η_{jj} distributions of the two-jet system for the processes $e^+e^- \to q\bar{q}A'$ (left panels) and $e^+e^- \to q\bar{q}\phi$ (middle panels) for several $\sqrt{s}$ and $m_{A'}$ (m_ϕ) without any kinematic cuts. Here, P_T^{jj} is the transverse momentum of the two-jet system and M_{jj} is the invariant mass, θ_{jj-z} is the angle between the momentum of the two-jet system and the particle beam axis, and η_{jj} is the rapidity of the two-jet system. For comparison, we use MadGraph [59] to analyze the kinematic distributions of the dominant background processes
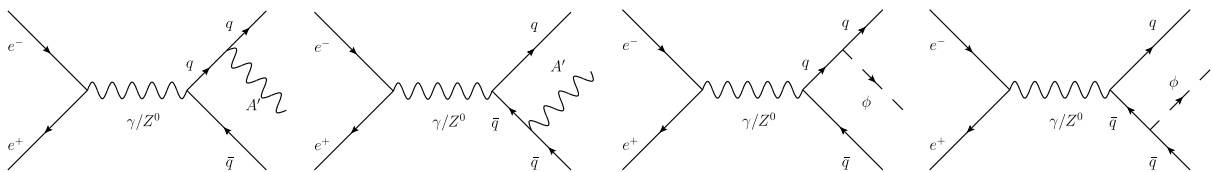

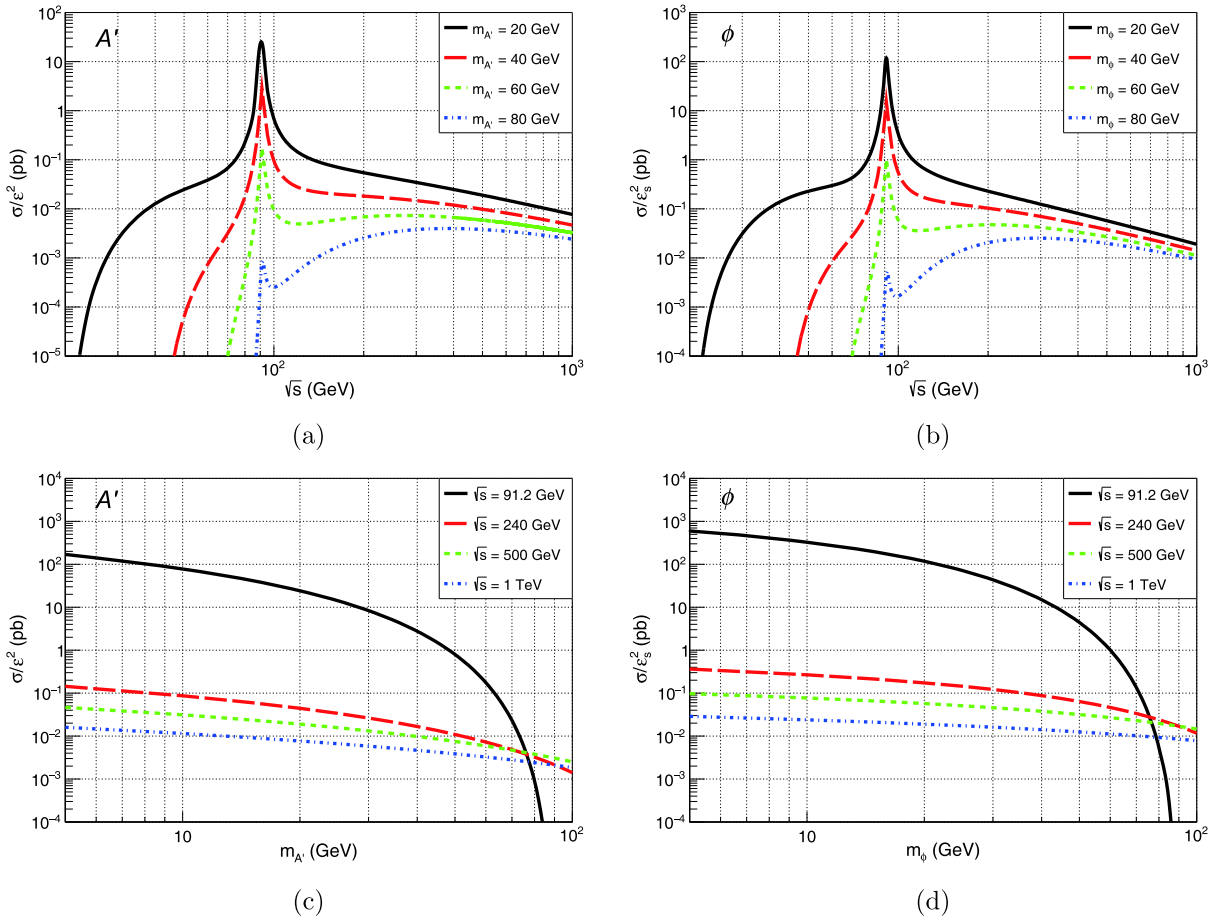Fig. 2.   The Feynman diagrams for the processes $e^+e^- \to q\bar{q}A'$ and $e^+e^- \to q\bar{q}\phi$.

Fig. 3.   (color online) Reduced cross-sections of the processes $e^+e^- \to q\bar{q}A'$ (left panels) and $e^+e^- \to q\bar{q}\phi$ (right panels) as function of $\sqrt{s}$ and $m_{A'}$ or m_ϕ.

$e^+e^- \to q\bar{q}\nu\bar{\nu}$ ($\nu = \nu_e$, ν_μ and ν_τ), which is shown in Fig. 4 (right panels). For $\sqrt{s} \geq 240$ GeV, the M_{jj} distributions of the background exhibit two peaks around $M_{jj} \approx 91$ GeV and 125 GeV due to the contributions of the resonant Z^0 and the Higgs boson. However, for $\sqrt{s} = 91.2$ GeV, the Z^0 peak is not obvious, because we have set the minimum transverse momentum of the jets to 0.5 GeV. From Fig. 4, one can see that the kinematic distributions of the two processes are somewhat different. We further investigate these distributions as function of $\cos\theta_{jj-z}$ and P_T^{jj} in Fig. 5 for several $\sqrt{s}$ and $m_{A'}$ (m_ϕ) values. Compared with the scalar mediator, the distributions for the dark photon A' are restricted to a smaller area. For example, for $\sqrt{s} = 91.2$ GeV, the dominant area for A' is $\cos\theta_{jj-z} \in (-1, -0.9)$ and $(0.9, 1)$ with $P_T^{jj} \in (0, 10)$, while the area for ϕ is comparatively broader. For higher center-of-mass energies $\sqrt{s}$, this trend is even more obvious.

As mentioned above, the kinematic distributions of the dark photon A' and dark scalar mediator ϕ are different. The difference can be enhanced by imposing appropriate kinematic cuts on the P_T^{jj} and $\cos\theta_{jj-z}$ distributions. As we show below, there are significant differences

between the production of the dark photon and dark scalar mediator at e^+e^- colliders.

In order to show the difference in P_T^{jj}, we impose a cut on $\cos\theta_{jj-z}$ such that $-0.9 < \cos\theta_{jj-z} < 0.9$, presented in Fig. 6. In the case of $\sqrt{s} = 91.2$ GeV and $m_{A'}(m_\phi) = 20$ GeV and for $18 \lesssim P_T^{jj} \lesssim 40$, the P_T^{jj} distributions of $e^+e^- \to q\bar{q}A'$ are attenuated as P_T^{jj} increases, while the P_T^{jj} distributions of $e^+e^- \to q\bar{q}\phi$ are substantially flat in this region. In the case of $\sqrt{s} = 1$ TeV and $m_{A'}(m_\phi) = 50$ GeV, the differences of the P_T^{jj} distributions of the two processes become much easier to identify. For $60 \lesssim P_T^{jj} \lesssim 460$, the P_T^{jj} distributions of $e^+e^- \to q\bar{q}A'$ are monotonically attenuated as P_T^{jj} increases. However, the P_T^{jj} distributions of $e^+e^- \to q\bar{q}\phi$ first increase quickly, and then decrease slowly in the same region. We also display the transverse momentum distributions of the background with the same cuts, which show quite a different shape for $\sqrt{s} = 91.2$ GeV.

As examples of $\cos\theta_{jj-z}$ distributions, we present in Fig. 7 the differential cross-sections of the two processes for $\sqrt{s} = 91.2$ GeV, 240 GeV, 500 GeV, 1 TeV and
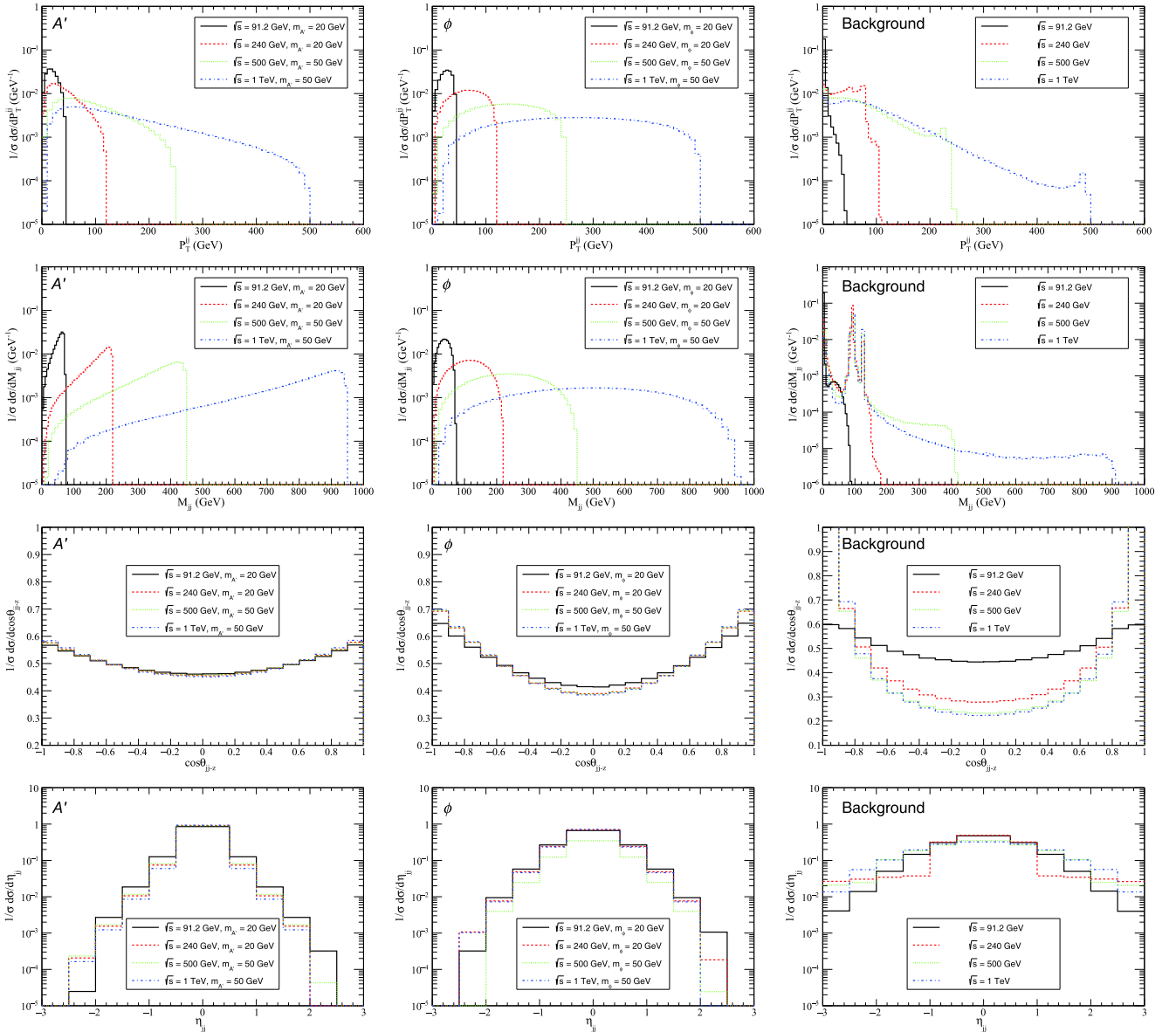
Fig. 4.   (color online) Normalized P_T^{jj}, M_{jj}, $\cos\theta_{jj-z}$ and η_{jj} distributions of the two-jet system for the dark photon production process $e^+e^- \to q\bar{q}A'$ (left panels), the dark scalar mediator production process $e^+e^- \to q\bar{q}\phi$ (middle panels), and the dominant background process $e^+e^- \to q\bar{q}\nu\bar{\nu}$ (right panels), for $\sqrt{s}$ = 91.2 GeV, 240 GeV, 500 GeV, and 1 TeV.

$m_{A'}(m_\phi)$ = 20 GeV or 50 GeV. It can be seen that the cuts of P_T^{jj} can enhance the difference between the dark photon and dark scalar mediator. Imposing the cuts $P_T^{jj} >$ 20, 50,100 and 240 GeV for the above center-of-mass energies, we find that the differential distributions of $e^+e^- \to q\bar{q}A'$ reach a maximum around $\cos\theta_{jj} = 0$, with the inverted "U" shape. However, for the scalar mediator, the maximum of the peak lies around $\cos\theta_{jj} = \pm 0.7$, and the shape looks like the letter "M". The shape of the angular distribution of the background with the same cuts varies dramatically for typical $\sqrt{s}$ values.

4   Identifying the dark photon signal against the background

Future e^+e^- colliders are expected to play a crucial role in discovering the nature of DM (dark sector) particles since they have a cleaner background. In this section, we focus on how to identify the heavy dark photon A' signal against the expected background at a future CEPC experiment. The analysis is similar for the dark scalar mediator ϕ . In the dark photon model of Eq. (1), A' can decay into a pair of SM quarks and a DM pair. The related decay widths are defined as
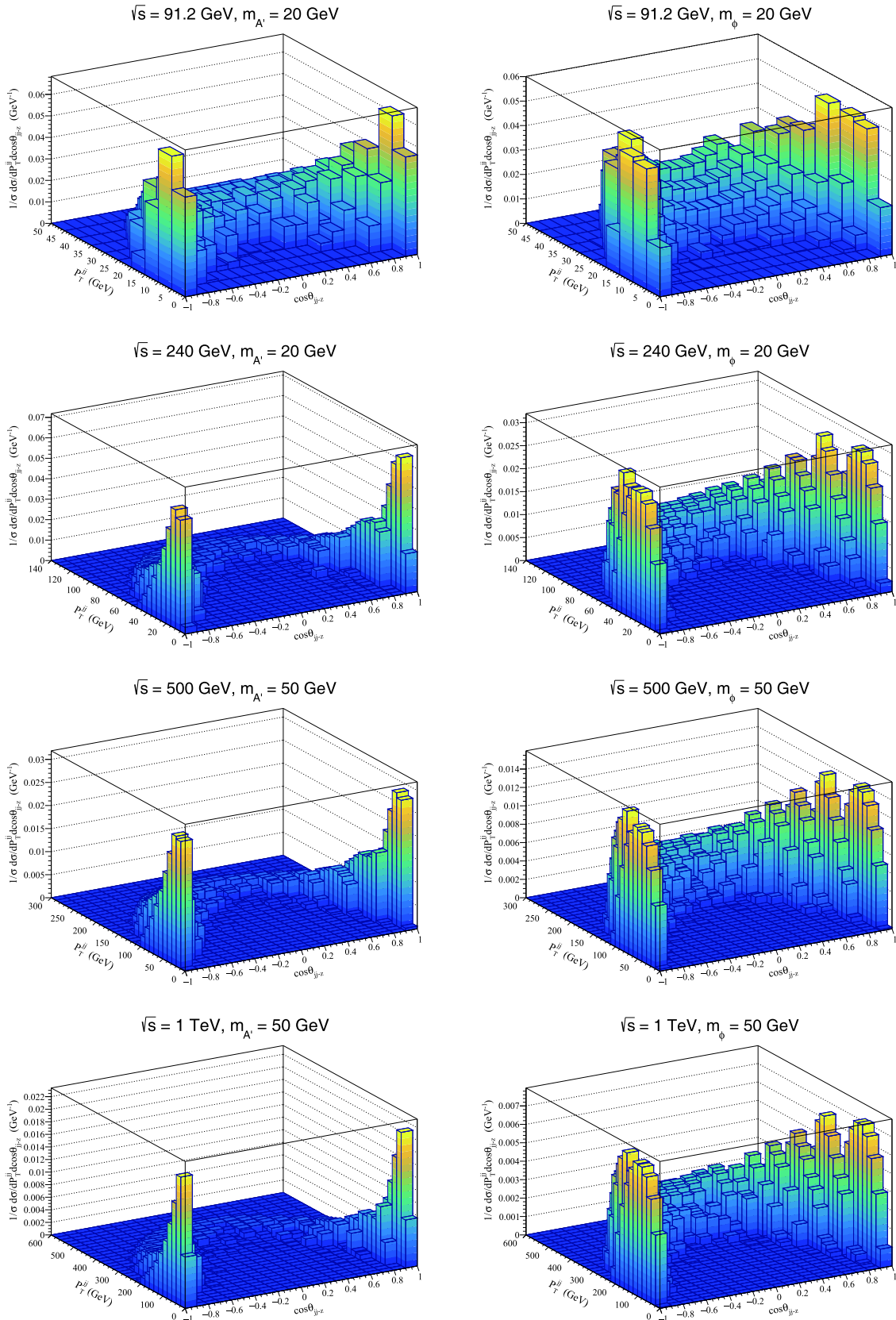
Fig. 5.　(color online) Normalized distributions as function of $\cos\theta_{jj-z}$ and P_T^{jj} for the processes $e^+e^- \to q\bar{q}A'$ (left panels) and $e^+e^- \to q\bar{q}\phi$ (right panels), for several $\sqrt{s}$ and $m_{A'}$ (m_ϕ) values without any kinematic cuts.
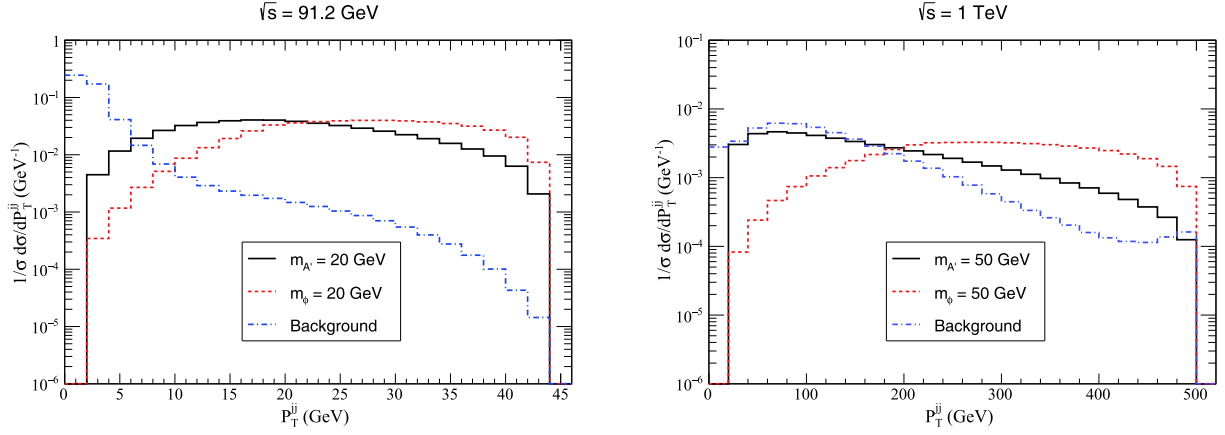
Fig. 6.   (color online) Normalized P_T^{jj} distributions of the two-jet system for the two processes and the background, for $\sqrt{s}$ = 91.2 GeV (left panel) and 1 TeV (right panel), with the cut $-0.9 < \cos\theta_{jj_z} < 0.9$.
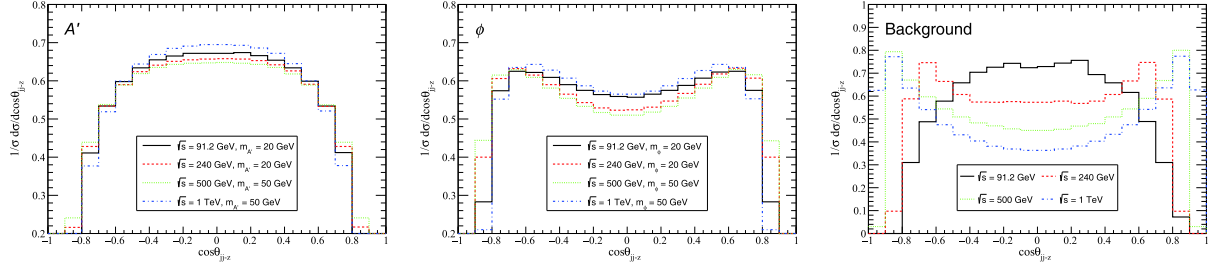

Fig. 7.   (color online) Normalized $\cos\theta_{jj}$ distributions of the two-jet system for the two processes and the background with cuts $P_T^{jj} >$ 20, 50,100 and 240 GeV, for $\sqrt{s}$ = 91.2 GeV, 240 GeV, 500 GeV and 1 TeV.

$$\Gamma(A' \to \chi\bar{\chi}) = \frac{g_\chi^2 (m_{A'}^2 + 2m_\chi^2)\sqrt{m_{A'}^2 - 4m_\chi^2}}{12\pi m_{A'}^2},$$

$$\sum_q \Gamma(A' \to q\bar{q}) = \sum_q \frac{\varepsilon^2 e^2 c_q^2 (m_{A'}^2 + 2m_q^2)\sqrt{m_{A'}^2 - 4m_q^2}}{4\pi m_{A'}^2}, \quad (5)$$

where c_q is the charge of the quarks. The branching ratio of $A' \to \chi\bar{\chi}$ can be written as

$$\mathrm{Br}(A' \to \chi\bar{\chi}) = \frac{\Gamma(A' \to \chi\bar{\chi})}{\Gamma(A' \to \chi\bar{\chi}) + \sum\limits_q (A' \to q\bar{q})}, \quad (6)$$

which is related to g_χ and ε, while the combined parameter $\alpha_\chi \varepsilon^2$ can be obtained from Fig. 1. Here we choose m_χ = 8.6 GeV, g_χ = 0.032, we extract ε from the XENON-1T curve in Fig. 1, and obtain the branching ratios of $A' \to \chi\bar{\chi}$ listed in Table 1. In the following, we study the $e^+e^- \to q\bar{q}A'$ process with $A' \to \chi\bar{\chi}$ due to its cleaner background. The dominant background process is $e^+e^- \to q\bar{q}\nu\bar{\nu}$ ($\nu = \nu_e, \nu_\mu,$ and ν_τ). In the final states of both the signal and background processes, we observe only two jets. The background process is simulated by Mad-Graph [59]. The invariant mass $M_{RA'}$ of the dark photon can be reconstructed from the recoil four-momentum of the two-jet system, where $M_{RA'}$ is defined as,

$$M_{RA'} = \sqrt{(p_{e^+} + p_{e^-} - p_{j1} - p_{j2})^2}, \quad (7)$$

where p_{e^+}, p_{e^-}, p_{j1} and p_{j2} are the four-momenta of the incoming electron, positron and the two jets in the final states, respectively. We focus on the light quark jets ($q = u, d, s, c$ and b) since the top quark decays quickly.

Theoretically, the on-shell dark photon events can be reconstructed precisely at $M_{RA'} = m_{A'}$ in the invariant mass spectrum. However, the detector has a finite energy resolution, which results in bump structures in the $M_{RA'}$ spectrum. To make our estimate more realistic, we simulate this effect by smearing the jet energies assuming a Gaussian resolution,

$$\frac{\delta(E)}{E} = \frac{A}{\sqrt{E}} \oplus B, \quad (8)$$

where $\delta(E)/E$ is the energy resolution, A is the sampling term, B a constant term, and $\oplus$ denotes the sum in quadrature. According to the CEPC CDR [41], the energy resolution for light jets ranges from 6% at E=20 GeV to 3.6% at E =100 GeV. We adopt the parameters A = 25.7% and B = 2.4%. The smearing effect is introduced in the same way in the reconstruction of the background events.

In order to identify the dark photon signal against the background, we need to impose proper kinematic cuts. The cuts are based on the kinematic distributions of the

Table 1.   The mixing parameter ε and the branching ratios of $A' \to \chi\bar{\chi}$ as function of the dark photon mass $m_{A'}$, for m_χ of 8.6 GeV and g_χ of 0.032.

$m_{A'}$	20 GeV	30 GeV	40 GeV	50 GeV	60 GeV
ε	0.0030	0.0067	0.012	0.019	0.027
Br($A' \to \chi\bar{\chi}$)	0.996	0.985	0.955	0.898	0.809

signal and background processes. We set the basic transverse momentum cut at $P_T > 10$ GeV and the rapidity cut at $|\eta_j| < 4$. In order to identify an isolated jet, the angular distribution between jets i and j is defined by

$$\triangle R_{ij} = \sqrt{\triangle\phi_{ij}^2 + \triangle\eta_{ij}^2}, \tag{9}$$

where $\triangle\phi_{ij}^2$ ($\triangle\eta_{ij}^2$) denotes the azimuthal angle (rapidity) difference between the two jets. In the two-jet system, we set the basic cut at $\triangle R > 0.4$ for both the signal and background processes.

In Fig. 8, we show the differential cross-section $d\sigma/dM_{RA'}$ as function of the invariant mass of the dark photon for $m_{A'} = 20, 30, 40, 50$ and 60 GeV, with the smearing and the above kinematic cuts. The reconstructed signal has a shape that complies with a Gaussian distribution with the expectation of $m_{A'}$ and the standard deviation of the energy resolution of $\delta(E)$. In contrast to the case of $\sqrt{s} = 91.2$ GeV, the signal at $\sqrt{s} = 240$ GeV has a wider spread since $\delta(E)$ is larger.

In order to identify the dark photon signal against the background, the significance of the signal-to-noise ratio needs to be explored. To enhance the significance, we impose the following cuts on the invariant mass spectrum: $|M_{RA'} - m_{A'}| < 6$ GeV at $\sqrt{s} = 91.2$ GeV, and $|M_{RA'} - m_{A'}| < 12$ GeV at $\sqrt{s} = 240$ GeV. For $\sqrt{s} = 91.2$ GeV and with the CEPC integrated luminosity of $\mathcal{L} = 2$ ab^{-1} and for several $m_{A'}$ values, we estimate the number of events for the signal (N_S) and background (N_B) processes, as well as the significance $S/\sqrt{B}$, as listed in Table 2. It can be seen that for $m_{A'} = 20, 30, 40$ and 50 GeV, the significance is

greater than 3σ.

In the case of the CEPC operating energy of $\sqrt{s} = 240$ GeV, we adopt a higher integrated luminosity of $\mathcal{L} = 20$ ab^{-1}. The number of events for the signal and background processes and the significance $S/\sqrt{B}$ are given in Table 3. In comparison with Table 2, we obtain a much smaller number of dark photon events. This is understandable since for 20 GeV < $m_{A'}$ < 60 GeV, the cross-section decreases with the center-of-mass energy for $\sqrt{s} > 91.2$ GeV, as demonstrated in Fig. 3 (a) and (c). In addition, we obtain many more background events for $\sqrt{s} = 240$ GeV than for $\sqrt{s} = 91.2$ GeV. This is due to the new topology of Feynman diagram for the background process shown in Fig. 9, whose contribution increases with $\sqrt{s}$. This topology is excluded in the signal since we assumed that the dark photon interacts only with quarks.

As an additional element relevant for a future CEPC experiment, we present the significance $S/\sqrt{B}$ versus the integrated luminosity for $\sqrt{s} = 91.2$ GeV and $\sqrt{s} = 240$ GeV in Fig. 10. In the case of $\sqrt{s} = 91.2$ GeV, the minimum integrated luminosities for the 3σ discovery of the dark photon with $m_{A'} = 20, 30, 40, 50$ and 60 GeV are 1.23, 0.490, 0.473, 0.971 and 6.67 ab^{-1}, respectively. Hence, it is understandable why the dark photon signal was not found at the Large Electron-Positron (LEP) collider, since the total luminosity of the LEP experiments [60] did not reach the minimum integrated luminosity for the 3σ discovery of the dark photon with 20 GeV< $m_{A'}$ < 60 GeV. At CEPC with $\sqrt{s} = 91.2$ GeV, the yearly luminosity is expected to be 4 ab^{-1}year^{-1} for a single interaction point (CEPC will have two interaction points), and it

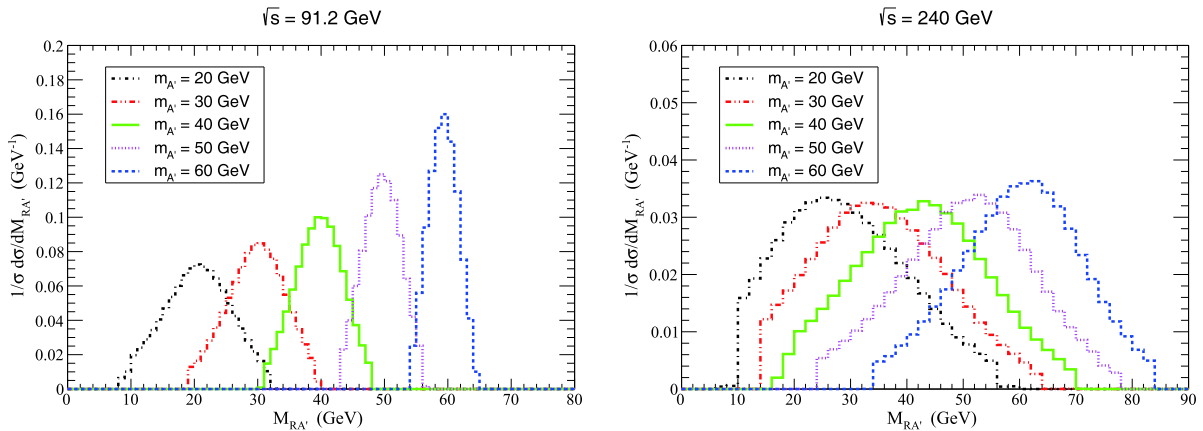
Fig. 8.   (color online) Normalized differential cross-section $d\sigma/dM_{RA'}$ as function of the invariant mass of the dark photon for $m_{A'} = 20$, 30, 40, 50 and 60 GeV, of the process $e^+e^- \to q\bar{q}A'$ for $\sqrt{s} = 91.2$ GeV (left panel) and $\sqrt{s} = 240$ GeV (right panel), with the smearing and proper kinematic cuts.

Table 2.   Number of events for the signal (N_S) and background (N_B) processes and the significance $S/\sqrt{B}$ for the integrated luminosity $\mathcal{L} = 2$ ab^{-1} at $\sqrt{s} =$91.2 GeV, with the smearing and proper kinematic cuts.

$m_{A'}$	20 GeV	30 GeV	40 GeV	50 GeV	60 GeV
N_S ($\mathcal{L} = 2$ ab^{-1})	191	368	372	206	46
N_B ($\mathcal{L} = 2$ ab^{-1})	2503	3697	3636	2304	799
$S/\sqrt{B}$	3.82	6.05	6.17	4.29	1.63

Table 3.   The same as Table 2, but for $\mathcal{L} = 20$ ab^{-1}, $\sqrt{s} =$240 GeV and $|M_{RA'} - m_{A'}| < 12$ GeV.

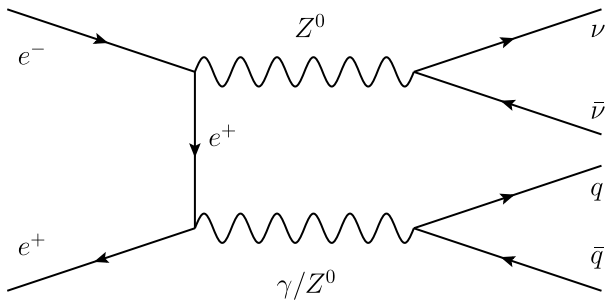| $m_{A'}$	20 GeV	30 GeV	40 GeV	50 GeV	60 GeV
N_S ($\mathcal{L} = 20$ ab^{-1})	2	10	23	39	53
N_B ($\mathcal{L} = 20$ ab^{-1})	60252	114953	210674	380295	682870
$S/\sqrt{B}$	0.00815	0.0295	0.0501	0.0632	0.0641

Fig. 9.   A possible topology of the Feynman diagram for the background, which is excluded for the signal process.

would be possible for a CEPC experiment to perform a decisive measurement of the dark photon (20 GeV$< m_{A'} <$ 60 GeV) in less than one operating year. In the case of $\sqrt{s} = 240$ GeV, the minimum integrated luminosities required for one signal event with the above $m_{A'}$ values are 7.06, 1.91, 0.853, 0.508 and 0.374 ab^{-1}, respectively. Therefore, with CEPC running at $\sqrt{s} = 240$ GeV and a luminosity of 0.4 ab^{-1}year^{-1} for a single interaction point, it would be hardly possible to get any signal of the dark

photon (20 GeV$< m_{A'} <$ 60 GeV) in one operating year.

5   Summary

The dark sector may consist of not only DM but also of one or more new force-carrying mediators which couple to the SM particles. We discussed the vector dark photon A' and the scalar mediator ϕ which could be produced in the processes $e^+e^- \to q\bar{q}A'$ and $e^+e^- \to q\bar{q}\phi$ at future e^+e^- colliders. The production cross-sections of these processes were predicted for $\sqrt{s} = 91.2$ GeV, 240 GeV, 500 GeV and 1 TeV. We further studied the kinematic distributions of the two-jet system in the final state, and found that they could be used to identify (or exclude) the dark photon and the dark scalar mediator, as well as to distinguish between them. In this work, we only considered the interaction between the dark photon and quarks, and with the process $e^+e^- \to q\bar{q}A'$ as an example, we investigated the discovery potential of the dark photon at CEPC with $\sqrt{s} = 91.2$ GeV and 240 GeV. It was shown that the dark photon with $m_{A'}$ ranging from 20 GeV to 60
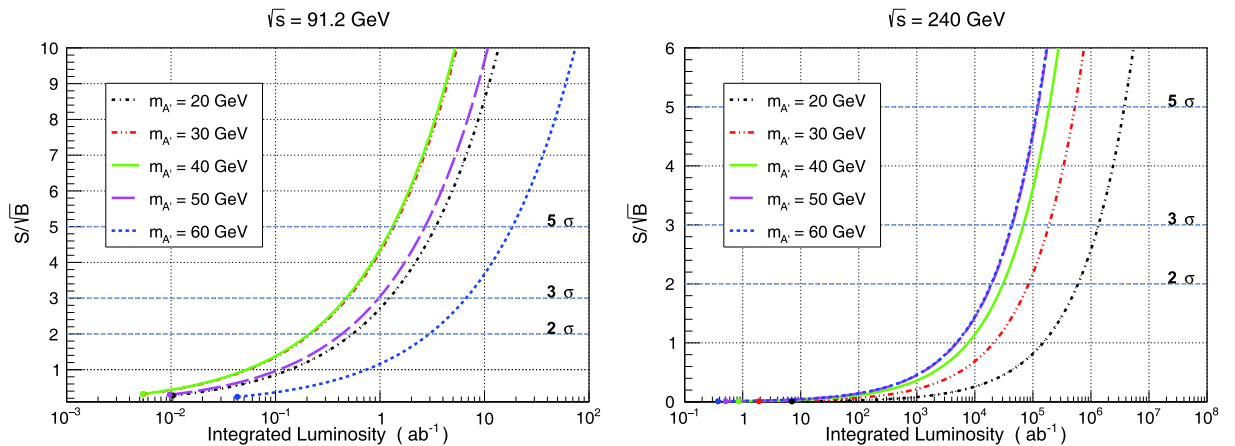
Fig. 10.   (color online) Significance versus integrated luminosity for $m_{A'} = 20$, 30, 40, 50 and 60 GeV, and $\sqrt{s} = 91.2$ GeV (left panel) and $\sqrt{s} = 240$ GeV (right panel). The dots represent the minimum integrated luminosity for one signal event.

GeV might be discovered in the process $e^+e^- \to q\bar{q}A'$ at e^+e^- colliders, e.g. at the super-Z factory or CEPC, with the minimum required integrated luminosity for the 3σ discovery of about 0.473~6.67 ab^{-1}. If the interaction between the dark mediator and leptons is also considered, $e^+e^- \to \ell^+\ell^- A'$ and $e^+e^- \to \gamma A'$ could be the other interesting processes to study, where the WW production would be the background. The method proposed in this work could also be used to search for any other invisible particles in e^+e^- annihilation.

References

1 N. Aghanim et al (Planck Collaboration), arXiv: 1807.06209[astro-ph.CO]
2 C. Conroy, A. Loeb, and D. Spergel, Astrophys. J., **741**: 72 (2011), arXiv:1010.5783[astro-ph.GA]
3 Y. Sofue and V. Rubin, Ann. Rev. Astron. Astrophys., **39**: 137 (2001), arXiv:astro-ph/0010594
4 S. Cole et al (2dFGRS Collaboration), Mon. Not. Roy. Astron. Soc., **362**: 505 (2005), arXiv:astro-ph/0501174
5 F. Beutler et al, Mon. Not. Roy. Astron. Soc., **416**: 3017 (2011), arXiv:1106.3366[astroph.CO]
6 L. Anderson et al, Mon. Not. Roy. Astron. Soc, **427**(4): 3435 (2013), arXiv:1203.6594[astro-ph.CO]
7 A. Vikhlinin et al, Astrophys. J., **692**: 1060 (2009), arXiv:0812.2720[astro-ph]
8 L. Fu et al, Astron. Astrophys., **479**: 9 (2008), arXiv:0712.0884[astro-ph]
9 R. Massey et al, Astrophys. J. Suppl., **172**: 239 (2007), arXiv:astro-ph/0701480
10 G. Jungman, M. Kamionkowski, and K. Griest, Phys. Rept., **267**: 195 (1996), arXiv:hep-ph/9506380
11 G. Bertone, D. Hooper, and J. Silk, Phys. Rept., **405**: 279 (2005), arXiv:hep-ph/0404175
12 T. Marrodn Undagoitia and L. Rauch, J. Phys. G, **43**(1): 013001 (2016), arXiv:1509.08767[physics.ins-det]
13 J. M. Gaskins, Contemp. Phys, **57**(4): 496 (2016), arXiv:1604.00014[astro-ph.HE]
14 F. Kahlhoefer, Int. J. Mod. Phys. A, **32**(13): 1730006 (2017), arXiv:1702.02430[hep-ph]
15 S. Tulin and H. B. Yu, Phys. Rept., **730**: 1 (2018), arXiv:1705.02358[hep-ph]
16 X. Chu, T. Hambye, and M. H. G. Tytgat, JCAP, **1205**: 034 (2012), arXiv:1112.0493[hep-ph]
17 J. A. Evans, S. Gori, and J. Shelton, JHEP, **1802**: 100 (2018), arXiv:1712.03974[hep-ph]
18 R. Essig et al, arXiv: 1311.0029[hep-ph]
19 J. Alexander et al, arXiv: 1608.08632[hep-ph]
20 M. Pospelov, A. Ritz, and M. B. Voloshin, Phys. Lett. B, **662**: 53 (2008), arXiv:0711.4866[hep-ph]
21 M. Dutra, M. Lindner, S. Profumo et al, JCAP, **1803**: 037 (2018), arXiv:1801.05447[hep-ph]
22 B. Holdom, Phys. Lett, **166B**: 196 (1986)
23 M. Pospelov, Phys. Rev. D, **80**: 095002 (2009), arXiv:0811.1030[hep-ph]
24 M. Cirelli, P. Panci, K. Petraki et al, JCAP, **1705**(05): 036 (1705), arXiv:1612.07295[hep-ph]
25 S. N. Gninenko, D. V. Kirpichnikov, M. M. Kirsanov et al, Phys. Lett. B, **782**: 406 (2018), arXiv:1712.05706[hep-ph]
26 D. Banerjee et al (NA64 Collaboration), Phys. Rev. D, **97**(7): 072002 (2018), arXiv:1710.00971[hep-ex]
27 S. Abrahamyan et al (APEX Collaboration), Phys. Rev. Lett., **107**: 191804 (2011), arXiv:1108.2750[hep-ex]
28 H. Merkel et al, Phys. Rev. Lett, **112**(22): 221802 (2014), arXiv:1404.5502[hep-ex]
29 A. Adare et al, Phys. Rev. C, **91**(3): 031901 (2015), arXiv:1409.0851[nucl-ex]
30 J. L. Feng, I. Galon, F. Kling et al, Phys. Rev. D, **97**(3): 035001 (2018), arXiv:1708.09389[hep-ph]
31 P. Ilten, J. Thaler, M. Williams et al, Phys. Rev. D, **92**(11): 115017 (2015), arXiv:1509.06765[hep-ph]
32 D. Curtin, R. Essig, S. Gori et al, JHEP, **1502**: 157 (2015), arXiv:1412.0018[hep-ph]
33 S. Chatrchyan et al (CMS Collaboration), JHEP, **1312**: 030 (2013), arXiv:1310.7291[hep-ex]
34 J. P. Lees et al (BaBar Collaboration), Phys. Rev. Lett, **119**(13): 131804 (2017), arXiv:1702.03327[hep-ex]
35 P. Fayet, Phys. Rev. D, **75**: 115017 (2007), arXiv:hep-ph/0702176[HEP-PH]
36 M. He, X. G. He, C. K. Huang et al, JHEP, **1803**: 139 (2018), arXiv:1712.09095[hep-ph]
37 J. Jiang, H. Yang, and C. F. Qiao, Eur. Phys. J. C, **79**(5): 404 (2019), arXiv:1810.05790[hep-ph]
38 A. Anastasi et al (KLOE-2 Collaboration), Phys. Lett. B, **757**: 356 (2016), arXiv:1603.06086[hep-ex]
39 P. Ilten, Y. Soreq, J. Thaler et al, Phys. Rev. Lett, **116**(25): 251803 (2016), arXiv:1603.08926[hep-ph]
40 V. Prasad (BESⅢ Collaboration), arXiv: 1907.12058[hep-ex]
41 J. B. Guimarães da Costa et al (CEPC Study Group), arXiv: 1811.10545[hep-ex]
42 H. Baer et al., arXiv: 1306.6352[hep-ph]
43 M. Bicer et al (TLEP Design Study Working Group), JHEP, **1401**: 164 (2014), arXiv:1308.6176[hep-ex]
44 H. Abramowicz et al (CLIC Detector and Physics Study Collaboration), arXiv: 1307.5288[hep-ex]
45 N. Fornengo, P. Panci, and M. Regis, Phys. Rev. D, **84**: 115002 (2011), arXiv:1108.4661[hep-ph]
46 M. Kaplinghat, S. Tulin, and H. B. Yu, Phys. Rev. D, **89**(3): 035009 (2014), arXiv:1310.7945[hep-ph]
47 R. H. Helm, Phys. Rev., **104**: 1466 (1956)
48 J. D. Lewin and P. F. Smith, Astropart. Phys., **6**: 87 (1996)
49 C. Y. Li, Z. G. Si, and Y. F. Zhou, Nucl. Phys. B, **945**: 114678 (2019), arXiv:1904.02193[hep-ph]
50 T. Li, S. Miao, and Y. F. Zhou, JCAP, **1503**: 032 (2015), arXiv:1412.6220[hep-ph]
51 R. Agnese et al (CDMS Collaboration), Phys. Rev. Lett, **111**(25): 251301 (2013), arXiv:1304.4279[hep-ex]
52 H. Jiang et al (CDEX Collaboration), Phys. Rev. Lett, **120**(24): 241301 (2018), arXiv:1802.09016[hep-ex]
53 A. Tan et al (PandaX-Ⅱ Collaboration), Phys. Rev. Lett, **117**(12): 121303 (2016), arXiv:1607.07400[hep-ex]
54 P. Agnes et al (DarkSide Collaboration), Phys. Rev. Lett, **121**(8): 081307 (2018), arXiv:1802.06994[astro-ph.HE]
55 E. Aprile et al (XENON Collaboration), Phys. Rev. Lett, **121**(11): 111302 (2018), arXiv:1805.12562[astro-ph.CO]
56 T. Hahn, Comput. Phys. Commun., **140**: 418 (2001), arXiv:hep-ph/0012260
57 V. Shtabovenko, R. Mertig, and F. Orellana, Comput. Phys. Commun., **207**: 432 (2016), arXiv:1601.01167[hep-ph]
58 T. Hahn, Comput. Phys. Commun., **207**: 341 (2016)
59 J. Alwall et al, JHEP, **1407**: 079 (2014), arXiv:1405.0301[hep-ph]
60 S. Schael et al (ALEPH and DELPHI and L3 and OPAL and SLD Collaborations and LEP Electroweak Working Group and SLD Electroweak Group and SLD Heavy Flavour Group), Phys. Rept., **427**: 257 (2006), arXiv:hep-ex/0509008